Self-diffusion in compressible gas flow through a microconduit

Di Shen and Kang Ping Chen*
School for Engineering of Matter, Transport, and Energy, Arizona State University, Tempe, Arizona 85287-6106, USA

(Received 10 October 2018; published 27 February 2019)

Steady viscous compressible gas flow through a microconduit is studied using the classical formulation of compressible Navier-Stokes equations with the no-slip condition. The mathematical theory of Klainerman and Majda for low Mach number flow is employed to derive asymptotic equations in the limit of small Mach number. The leading-order equations give rise to the Hagen-Poiseuille solution, and the equations at a higher order lead to a diffusive velocity field induced by self-diffusion of the gas. An explicit solution for the diffusive field is obtained under the no-slip condition and the overall flow exhibits a sliplike mass flow rate even though the velocity satisfies the no-slip condition. The results indicate that the classical formulation includes the self-diffusion effect and it embeds the extended Navier-Stokes equation (ENSE) theory without the need of introducing an additional constitutive hypothesis or assuming slip on the boundary. The predicted pressure profile agrees well with experiments. Contrary to reports in many ENSE publications, an extensive comparison with 35 experiments shows that in the slip-flow regime the predicted mass flow rate is still significantly below the measured mass flow rate, as the self-diffusion effect is too small to account for the observed mass flow-rate enhancement in this flow regime.

DOI: 10.1103/PhysRevFluids.4.024202

I. INTRODUCTION

Rapid growing applications of micromechanical systems (MEMS) and microfluidics during the past three decades have stimulated significant research on viscous compressible flow through micron-size conduits [1–6]. Steady compressible flow of a gas through such a microconduit can produce a mass flow rate much higher than that predicted by the classical Hagen-Poiseuille solution for macroscale flows [7–21]. This departure from the classical result has been attributed to a breakdown of the continuum assumption, which is the basis for the Navier-Stokes equations for macroscale flows. The mean free path in a low-pressure gas flow through a microconduit can become comparable to the characteristic length of the confining geometry [16,22,23] and a large surface-to-volume ratio can make the interaction between the wall and the gas important for the flow. The degree of departure of such a small scale flow from the classical continuum theory is commonly characterized by the Knudsen number, $\mathrm{Kn} = \lambda/L_c$, with λ being the mean free path of the gas molecules and L_c being the characteristic length of the flow (typically the hydraulic diameter of the conduit). It is widely acknowledged that for Knudsen number $\mathrm{Kn} < 0.001$ the classical continuum formulation of the Navier-Stokes equations with the no-slip condition holds, and when $\mathrm{Kn} > 10$ free molecular flow (Knudsen diffusion) results [8,24,25]. Thus, as the Knudsen number is increased from a very small value to a large value, the flow changes from a continuum flow to a free molecular flow. The flow regimes between the continuum limit and the free molecular

*Corresponding author: k.p.chen@asu.edu

flow limit are commonly classified as the slip-flow regime, the transitional-flow regime, etc., in the order of increasing Knudsen number. For example, gas flows through MEMS devices typically have Knudsen numbers in the range of 0.01 to 1, which fall into the slip and the transitional flow regimes, corresponding to $0.001 < \mathrm{Kn} < 0.1$ and $0.1 < \mathrm{Kn} < 10$, respectively [16]. Flow in the slip regime, however, is expected to show only a small to moderate departure from the classical continuum theory, as the Knudsen number is still relatively small. It has been common to assume that in the slip-flow regime the breakdown of the continuum theory occurs only in the Knudsen layer adjacent to the solid boundary and the Navier-Stokes equations still hold in the bulk of the fluid. Within the Knudsen layer, which has a thickness in the order of the mean free path, gas-wall collision is more frequent than intramolecular collision. This results in a sliplike thin layer, which has been often modeled by a slip-boundary condition for the gas motion in the bulk [7,26–31]. The results from this slip-boundary-condition approach for the slip-flow regime match well with experimentally observed mass flow rate when a slip parameter is tuned to a suitable value. Another popular approach to compressible microflow in the slip-flow regime is the extended Navier-Stokes equation (ENSE) theory formulation proposed by Brenner [32] and Durst *et al.* [33]. This approach recognizes the importance of self-diffusion (bulk diffusion) caused by a local-density gradient in compressible flow through small conduits [34] and it extends the Navier-Stokes equations to include an additional diffusive mass (or volume) flux from self-diffusion (mass or volume) as well as an additional diffusive momentum flux. The overall velocity is assumed to be given by the sum of the convective velocity, as in the Navier-Stokes equations, and a diffusive velocity from the self-diffusion of the fluid mass. Only the convective velocity is made to satisfy the no-slip condition while the diffusive velocity is allowed to slip on the wall [32,33,35–39]. Noticeably, this ENSE approach involves constitutive modifications to both the mass flux and the stress tensor of the classical Newtonian fluid. Many ENSE publications have reported that this approach yields good agreements with experiments without an adjusting parameter, which has been advocated as a major appeal of this approach. The difference between the slip-boundary-condition approach and ENSE is that the former lacks the self-diffusion mechanism in the bulk and it also uses an adjustable slip parameter. It is also noted that Veltzke and Thaming [40] used a slightly different approach by simply superposing Knudsen diffusion upon the Hagen-Poiseuille flow with a linear pressure profile. The velocity associated with the Knudsen diffusion flux still slips on the wall. They have also produced good agreements with their own experimental measurements. Other approaches that have been successfully applied to the same range as well as higher Knudsen numbers include linearized Boltzmann equations, direct simulation Monte Carlo, etc. [29,41–43]. Together, these studies have significantly advanced our understanding of compressible flow through microconduits.

The cornerstone of the ENSE theory is the inclusion of the self-diffusion effect for a viscous compressible flow. It cites the lack of the self-diffusion mechanism in the classical formulation of the Navier-Stokes equations as the motivation for the development of the extended theory. Using the classical formulation of the Navier-Stokes equations with the no-slip condition, we have recently found that the mass flow rate for the volumetric-expansion-driven *transient* drainage flow of a viscous compressible fluid from a semisealed microcapillary is diffusive and it is proportional to the square of the tube radius [44,45]. Noticeably, the sliplike mass flow rate is the result of the longitudinal mass diffusion caused by a local-density gradient, consistent with the self-diffusion effect modeled in the ENSE theory for *steady* flows. The result for the drainage flow, however, is strictly derived from the linearized compressible Navier-Stokes equations *without any additional hypothesis*, and the velocity for the drainage flow satisfies the no-slip condition on the capillary wall. This finding naturally raises the following questions:

(a) Is the fluid's self-diffusion effect already embedded in the classical formulation for both transient and steady flows?

(b) Does the classical formulation also admit no-slip solutions with sliplike mass flow rates for *steady* compressible flow through narrow conduits?

(c) If such a steady sliplike solution exists, how does it perform compared to experiments?

To answer these questions, we revisit the problem of steady compressible gas flow through a long and narrow open microconduit (circular tube or two-dimensional channel) within the framework of the classical formulation of the compressible Navier-Stokes equations with the no-slip condition. The mathematical theory for low Mach number flows developed by Klainerman and Majda [46,47] is employed to expand the governing equations in terms of the vanishing Mach number and to derive asymptotic equations for compressible flow through microconduits. It will be shown that for a compressible flow in a long and narrow open conduit the leading-order equations give rise to the Hagen-Poiseuille solution, and the balance between the convective acceleration and an equivalent body force induced by a local-density gradient at the next order leads to a steady diffusive field. The cross-sectional averaged mass flux of the diffusive field will be shown to obey Fick's law of diffusion, which gives rise to the self-diffusion effect. The Helmholtz decomposition theorem is then used to obtain an explicit solution for the diffusive field under the no-slip condition. The mass flow rate of the microflow is the sum of the mass flow rate from the Hagen-Poiseuille flow and that due to the diffusive field, which is identical to that from the ENSE theory when adjusted for the contribution of the bulk viscosity. This paper shows that the classical formulation already embeds the self-diffusion effect and the ENSE theory without the need of introducing an additional constitutive hypothesis or assuming slip on the boundary. For a very narrow conduit, the self-diffusion effect dominates, and the mass flow rate is sliplike with a radius-square dependence, even though the velocity satisfies the no-slip condition. These results are compared to multiple experiments and other works published in the literature. The pressure profile agrees very well with measured data. Contrary to the claims made in many ENSE publications, however, in the slip-flow regime, the predicted mass flow rate is still significantly below the measured mass flow rate, as the self-diffusion effect is too small to account for the observed mass flow-rate deviation from the Hagen-Poiseuille solution in this flow regime.

II. SELF-DIFFUSION EMBEDDED IN THE COMPRESSIBLE NAVIER-STOKES EQUATIONS

The conservative forms of the continuity and the compressible Navier-Stokes equations [48] are

$$\frac{\partial \rho}{\partial t} + \nabla \cdot (\rho \mathbf{v}) = 0, \tag{2.1}$$

$$\frac{\partial (\rho \mathbf{v})}{\partial t} + \nabla \cdot (\rho \mathbf{v} \otimes \mathbf{v}) = -\nabla p + (\mu_b + \mu/3)\nabla(\nabla \cdot \mathbf{v}) + \mu \nabla^2 \mathbf{v}, \tag{2.2}$$

where ρ, p, and $\mathbf{v}$ are the density, pressure, and velocity of the fluid; μ_b is the bulk viscosity; and μ is the shear viscosity. An equation of state such as the ideal gas law is supplied to link the pressure and the density. Since compressible flows through microconduits are low Mach number flows (global Mach number $M \ll 1$), the energy equation is not included here as temperature change is assumed to be small. This assumption is adopted in most studies on microflows. In the following, we will show how self-diffusion arises from these governing equations for compressible flow through a long and narrow microconduit.

A. Self-diffusion in transient flow perturbing an equilibrium state

For a flow perturbing an equilibrium state, linearization of Eqs. (2.1) and (2.2) leads to the well-known linear acoustic equations governing the propagation of small amplitude acoustic waves [49,50]:

$$\frac{\partial \rho'}{\partial t} + \rho_0 \nabla \cdot \mathbf{v}' = 0, \tag{2.3}$$

$$\rho_0 \frac{\partial \mathbf{v}'}{\partial t} = -\nabla p' + (\mu_b + 4\mu/3)\nabla(\nabla \cdot \mathbf{v}') - \mu \nabla \times (\nabla \times \mathbf{v}'), \tag{2.4}$$

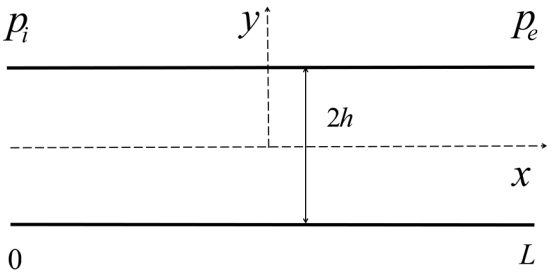

FIG. 1. Microflow through a channel. For a microcapillary, the radius of the capillary is R.

where $\rho' = \rho - \rho_0$ is the density perturbation from the equilibrium density ρ_0, p' is the pressure perturbation, and $\mathbf{v}'$ is the velocity. Density perturbation satisfies a damped wave equation of the form [49,51,52]

$$\frac{\partial^2 \rho'}{\partial t^2} = \left(c^2 + D_0 \frac{\partial}{\partial t}\right) \nabla^2 \rho', \tag{2.5}$$

where c is the speed of sound and

$$D_0 = (\mu_b/\mu + 4/3)\frac{\mu}{\rho_0} \tag{2.6}$$

is the damping coefficient for the density wave. The damping term in Eq. (2.5) is called "sound-absorption" in the acoustic literature [53].

For transient flows in semisealed long and narrow capillaries (Fig. 1), it is shown that density relaxes quickly in the transverse direction and it becomes uniform in the cross section shortly after startup [44]. Thus, $\rho = \rho(x, t)$, with x being the longitudinal direction. The second term on the right-hand side (rhs) of Eq. (2.4) then becomes $-\mathbf{e}_x D_0 \partial^2 \rho'/\partial x \partial t$, where $\mathbf{e}_x$ is the unit base vector in the x direction. This leads to the damping of the acoustic wave by the second term on the rhs of Eq. (2.5), which is due to the self-diffusion induced by the local-density gradient $\partial \rho'/\partial x$. Since Eq. (2.5) is derived from the linearized compressible Navier-Stokes equations, we conclude that the linearized compressible Navier-Stokes equations include the self-diffusion effect for transient flows via sound absorption.

B. Self-diffusion in steady flow through a microconduit

Consider the motion of a compressible fluid through a circular capillary with radius R and length L (Fig. 1). The capillary is long and narrow such that $R \ll L$. Steady-state flow is the long-time solution of a startup flow. The self-diffusion effect in a transient startup flow does not vanish at large times, as the dilatation $\nabla \cdot \mathbf{v}$ term in Eq. (2.2) remains in the momentum equation for steady compressible flows. The mathematical theory for low Mach number flows developed by Klainerman and Majda [46,47] can be employed to show that self-diffusion is persistent for steady compressible flow through a small capillary.

To this end, the governing Eqs. (2.1) and (2.2) are first made dimensionless with the scales used by Klainerman and Majda [47]. Let $\mathrm{v}_{\mathrm{ref}}$ be a reference fluid particle velocity, let L_{ref} be a reference length, and let a reference time be defined as $t_{\mathrm{ref}} = L_{\mathrm{ref}}/\mathrm{v}_{\mathrm{ref}}$. The reference pressure and density are p_{ref} and ρ_{ref}, respectively. A reference speed of sound can be defined as $c_{\mathrm{ref}} = \sqrt{p_{\mathrm{ref}}/\rho_{\mathrm{ref}}}$ (a constant factor is dropped for convenience; see Ref. [47]). The dimensionless velocity, pressure, density, coordinates, and time are $\bar{\mathbf{v}} = \mathbf{v}/v_{\mathrm{ref}}$, $\bar{p} = p/p_{\mathrm{ref}}$, $\bar{\rho} = \rho/\rho_{\mathrm{ref}}$, $\bar{\mathbf{x}} = \mathbf{x}/L_{\mathrm{ref}}$, and $\bar{t} = t/t_{\mathrm{ref}}$. A global

Mach number is defined as $M = \mathrm{v}_{\mathrm{ref}}/c_{\mathrm{ref}}$ and a Reynolds number is defined as $\mathrm{Re} = \rho_{\mathrm{ref}}\mathrm{v}_{\mathrm{ref}}L_{\mathrm{ref}}/\mu$, both of which are assumed to be small. The dimensionless governing equations are then

$$\frac{\partial\bar{\rho}}{\partial\bar{t}} + \bar{\nabla}\cdot(\bar{\rho}\bar{\mathbf{v}}) = 0, \tag{2.7}$$

$$\frac{\partial(\bar{\rho}\bar{\mathbf{v}})}{\partial\bar{t}} + \bar{\nabla}\cdot(\bar{\rho}\bar{\mathbf{v}}\otimes\bar{\mathbf{v}}) = -\frac{1}{M^2}\bar{\nabla}\bar{p} + \frac{\mu_b/\mu + 1/3}{\mathrm{Re}}\bar{\nabla}(\bar{\nabla}\cdot\bar{\mathbf{v}}) + \frac{1}{\mathrm{Re}}\bar{\nabla}^2\bar{\mathbf{v}}. \tag{2.8}$$

It is known that the limit of $M \to 0$ is singular as these governing equations change types [46]. For inviscid isentropic flows, Klainerman and Majda [47] have rigorously proved that for given initial data the linearized acoustics is a *uniformly* valid principal correction in the deviation of the compressible flow solution from the incompressible solution as the global Mach number $M \to 0$, and they have derived the following asymptotic results:

$$|\bar{\mathbf{v}} - (\bar{\mathbf{v}}^I + M\,\tilde{\mathbf{v}}^A)| \leqslant \Delta_5 M^2, \tag{2.9}$$

$$|\bar{p} - (\bar{p}_0 + M^2(\tilde{p}^I + \tilde{p}^A))| \leqslant \Delta_6 M^3, \tag{2.10}$$

where $||$ stands for the magnitude; superscripts I and A stand for incompressible and acoustic quantities, respectively; $\Delta_5 > 0$ and $\Delta_6 > 0$ are fixed constants; and $\bar{p}_0$ is a background thermodynamic pressure. The asymptotic results (2.9) and (2.10) have been extended by Klein [54] to nonisentropic flows and by Munz *et al.* [55,56] to the general heat conducting viscous compressible Navier-Stokes equations. These asymptotic results allow us to decompose a low Mach number flow into the sum of two fields, the limiting incompressible field and a linearized acoustic field, $\bar{\mathbf{v}} = \bar{\mathbf{v}}^I + \bar{\mathbf{v}}^A + O(M^2)$ with $\bar{\nabla}\cdot\bar{\mathbf{v}}^I = 0$ and $\bar{\mathbf{v}}^I = \lim_{M\to 0}\bar{\mathbf{v}}$. Specifically,

$$\bar{\mathbf{v}} = \bar{\mathbf{v}}^I + \bar{\mathbf{v}}^A + O(M^2) = \bar{\mathbf{v}}^I + M\,\tilde{\mathbf{v}}^A + O(M^2), \tag{2.11}$$

$$\bar{p} - \bar{p}_0 = \bar{p}^I + \bar{p}^A + O(M^3) = M^2\tilde{p}^I + M^2\tilde{p}^A + O(M^3). \tag{2.12}$$

Density can also be expanded:

$$\bar{\rho} = 1 + M^2\tilde{\rho}_2 + O(M^4). \tag{2.13}$$

These asymptotic expansions are valid for all times. In the absence of a continuous acoustic excitation and flow instabilities, a condition met by low Reynolds number steady microflows, the two flow fields are expected to approach steady-state solutions at large times which are governed by the corresponding steady-state equations:

$$\bar{\nabla}\cdot(\bar{\rho}\bar{\mathbf{v}}) = 0, \tag{2.14}$$

$$\bar{\nabla}\cdot(\bar{\rho}\bar{\mathbf{v}}\otimes\bar{\mathbf{v}}) = -\frac{1}{M^2}\bar{\nabla}\bar{p} + \frac{\mu_b/\mu + 4/3}{\mathrm{Re}}\bar{\nabla}(\bar{\nabla}\cdot\bar{\mathbf{v}}) - \frac{1}{\mathrm{Re}}\bar{\nabla}\times(\bar{\nabla}\times\bar{\mathbf{v}}), \tag{2.15}$$

where the vector identity $\nabla^2\mathbf{a} = \nabla(\nabla\cdot\mathbf{a}) - \nabla\times(\nabla\times\mathbf{a})$ has been used.

For steady flows, we replace the superscript A by D in the expansion (2.11) and (2.12), with

$$\bar{\mathbf{v}}^D = \lim_{t\to\infty}\bar{\mathbf{v}}^A, \quad \bar{p}^D = \lim_{t\to\infty}\bar{p}^A, \tag{2.16}$$

while maintaining the superscript I for the limiting steady incompressible field. Thus, for steady flows,

$$\bar{\mathbf{v}} = \bar{\mathbf{v}}^I + \bar{\mathbf{v}}^D + O(M^2) = \bar{\mathbf{v}}^I + M\ \tilde{\mathbf{v}}^D + O(M^2), \tag{2.17}$$

$$\bar{p} - \bar{p}_0 = \bar{p}^I + \bar{p}^D + O(M^3) = M^2\tilde{p}^I + M^2\tilde{p}^D + O\ (M^3). \tag{2.18}$$

The momentum equation for the limiting incompressible flow is (with $\bar{\rho} = 1$)

$$\bar{\nabla} \cdot (\bar{\mathbf{v}}^I \otimes \bar{\mathbf{v}}^I) = -\bar{\nabla}\tilde{p}^I - \frac{1}{\mathrm{Re}}\bar{\nabla} \times (\bar{\nabla} \times \bar{\mathbf{v}}^I). \tag{2.19}$$

Subtracting Eq. (2.19) from Eq. (2.15) and substituting Eqs. (2.17) and (2.18) into the result gives

$$\bar{\nabla} \cdot (\bar{\rho}\bar{\mathbf{v}} \otimes \bar{\mathbf{v}}) - \bar{\nabla} \cdot (\bar{\mathbf{v}}^I \otimes \bar{\mathbf{v}}^I) = -\bar{\nabla}\tilde{p}^D + \frac{\mu_b/\mu + 4/3}{\mathrm{Re}}\bar{\nabla}(\bar{\nabla} \cdot \bar{\mathbf{v}}^D) - \frac{1}{\mathrm{Re}}\bar{\nabla} \times (\bar{\nabla} \times \bar{\mathbf{v}}^D), \tag{2.20}$$

where for each of the three contributions on the right-hand side only the leading-order term has been retained. The limiting incompressible field $\bar{\mathbf{v}}^I$ is driven by the pressure gradient while the compressible field $\bar{\mathbf{v}}^D$ is driven by the density gradient. Since microflows are weak flows with very low mass flow rates, we seek a leading-order solution that is linear in each driving mechanism (gradient), which takes the form

$$\bar{\mathbf{v}}^I = \tilde{\mathbf{v}}_p\frac{\partial \bar{p}}{\partial \bar{x}}, \quad \bar{\mathbf{v}}^D = \tilde{\mathbf{v}}_\rho\frac{\partial \bar{\rho}}{\partial \bar{x}}, \tag{2.21}$$

and we neglect any interactive term that involves the product of the two velocities, i.e., the product of the two gradients, in the governing equations. Thus, there is no coupling between the incompressible field $\bar{\mathbf{v}}^I$ and the compressible field $\bar{\mathbf{v}}^D$ other than conservation of the overall mass. This approximation is used either explicitly or implicitly in all models involving density gradient for compressible microflows, for example the diffusive flux theories, and it puts the two flow driving mechanisms on equal footings.

With the assumption (2.21) and the density expansion (2.13), after neglecting the product term $\frac{\partial \bar{p}}{\partial \bar{x}}\frac{\partial \bar{\rho}}{\partial \bar{x}}$, Eq. (2.20) becomes

$$\bar{\nabla} \cdot (\bar{\rho}\bar{\mathbf{v}}^D \otimes \bar{\mathbf{v}}^D) = -\bar{\nabla}\tilde{p}^D + \frac{\mu_b/\mu + 4/3}{\mathrm{Re}}\bar{\nabla}(\bar{\nabla} \cdot \bar{\mathbf{v}}^D) - \frac{1}{\mathrm{Re}}\bar{\nabla} \times (\bar{\nabla} \times \bar{\mathbf{v}}^D). \tag{2.22}$$

The Helmholtz decomposition [57–59] can be used to further decompose $\bar{\mathbf{v}}^D = M\ \tilde{\mathbf{v}}^D$ to the sum of an irrotational part and a solenoidal part:

$$\tilde{\mathbf{v}}^D = \tilde{\mathbf{v}}^{IR} + \tilde{\mathbf{v}}^{RT}, \tag{2.23}$$

where $\nabla \times \tilde{\mathbf{v}}^{IR} = 0$, $\tilde{\mathbf{v}}^{IR} = \nabla\Phi$, and $\nabla \cdot \tilde{\mathbf{v}}^{RT} = 0$. Φ is the scalar velocity potential for the irrotational velocity. Thus, $\bar{\nabla} \times \tilde{\mathbf{v}}^D = \bar{\nabla} \times \tilde{\mathbf{v}}^{RT}$ and the momentum Eq. (2.22) becomes

$$M^2\bar{\nabla} \cdot (\tilde{\mathbf{v}}^D \otimes \tilde{\mathbf{v}}^D) + O(M^4) = -\bar{\nabla}\tilde{p}^D - \frac{\mu_b/\mu + 4/3}{\mathrm{Re}}M^3\bar{\nabla}(\tilde{\mathbf{v}}^D \cdot \bar{\nabla}\tilde{\rho}_2) - \frac{M}{\mathrm{Re}}\bar{\nabla} \times (\bar{\nabla} \times \tilde{\mathbf{v}}^{RT}), \tag{2.24}$$

where the continuity equation

$$\bar{\nabla} \cdot \bar{\mathbf{v}}^D = -\bar{\mathbf{v}}^D \cdot \bar{\nabla} \ln \bar{\rho} \tag{2.25}$$

has been used. For microflows through an open conduit with small to moderate ratios between the inlet pressure and the outlet pressure, Ref. [20] has shown that $M \sim \mathrm{Re} \sim \varepsilon = R/L$. Thus,

$M/\mathrm{Re} = O(1)$. Therefore, in the limit of $M \to 0$, the order $O(1)$ and $O(M^2)$ equations of Eq. (2.24) become, respectively,

$$-\bar{\nabla}\tilde{p}^D - \frac{M}{\mathrm{Re}}\bar{\nabla} \times (\bar{\nabla} \times \tilde{\mathbf{v}}^{RT}) = 0, \tag{2.26}$$

$$\bar{\nabla} \cdot (\tilde{\mathbf{v}}^D \otimes \tilde{\mathbf{v}}^D) = -(\mu_b/\mu + 4/3)\frac{M}{\mathrm{Re}}\bar{\nabla}(\tilde{\mathbf{v}}^D \cdot \bar{\nabla}\tilde{\rho}_2). \tag{2.27}$$

In dimensional forms, the solenoidal part of the diffusive velocity is then governed by the incompressibility and the creeping flow equations:

$$\nabla \cdot \mathbf{v}^{RT} = 0, \tag{2.28}$$

$$-\nabla p^D + \mu\nabla^2\mathbf{v}^{RT} = 0. \tag{2.29}$$

As will be shown in Sec. III below, the solenoidal velocity is induced by the irrotational part of the diffusive velocity and its role is to ensure that the diffusive velocity satisfies the no-slip condition on the wall.

Equation (2.27) reflects a balance between the convective acceleration and an equivalent body force induced by the self-diffusion of the fluid mass. It is noticed that, with a difference of a term of the higher-order $O(M^4)$, Eq. (2.27) is the same as the equation

$$\bar{\nabla} \cdot (\bar{\rho}\bar{\mathbf{v}}^D \otimes \bar{\mathbf{v}}^D) = -\frac{\mu_b/\mu + 4/3}{\mathrm{Re}}\bar{\nabla}(\bar{\mathbf{v}}^D \cdot \bar{\nabla}\ln\bar{\rho}), \tag{2.30}$$

which in dimensional form is

$$\nabla \cdot (\rho\mathbf{v}^D \otimes \mathbf{v}^D) = -(\mu_b + 4\mu/3)\nabla(\mathbf{v}^D \cdot \nabla\ln\rho). \tag{2.31}$$

It is observed that deviation of a compressible gas flow from the Hagen-Poiseuille solution stems from the continuous volumetric expansion of the gas along the conduit (rarefication effect), which makes the flow a developing flow instead of a fully developed flow. This effect is characterized by the convective acceleration of the fluid, which is balanced by the density gradient induced body force as shown by Eq. (2.31).

In a cylindrical coordinate, the velocity for an axisymmetric flow is given by $\mathbf{v} = \mathbf{e}_r \mathrm{v}_r(r,x) + \mathbf{e}_x \mathrm{v}_x(r,x)$, where $\mathbf{e}_r$ and $\mathbf{e}_x$ are the unit base vectors in the r and x directions, respectively. Density relaxes for compressible flow in long and narrow capillaries and it is a function of x only [44]:

$$\mathbf{v}^D \cdot \nabla\ln\rho = \mathrm{v}_x^D\frac{d}{dx}\ln\rho. \tag{2.32}$$

The x-direction component of Eq. (2.31) is

$$\frac{2}{r}\frac{\partial}{\partial r}\left(\rho r \mathrm{v}_r^D \mathrm{v}_x^D\right) + \frac{\partial}{\partial x}\left(\rho \mathrm{v}_x^D \mathrm{v}_x^D\right) = -(\mu_b + 4\mu/3)\frac{\partial}{\partial x}\left(\mathrm{v}_x^D\frac{d}{dx}\ln\rho\right). \tag{2.33}$$

This is the momentum balance equation at a length scale comparable to the length of the tube. At this long length scale, density gradient drives a large-scale compressible flow, which is decoupled from the incompressible field $\bar{\mathbf{v}}^I$ when the leading-order approximation (2.21) is adopted. Integrating Eq. (2.33) over the cross section and utilizing the no-penetration condition for v_r^D on the tube wall gives

$$\frac{\partial}{\partial x}\int_0^R 2\pi r\rho\left(\mathrm{v}_x^D\right)^2 dr = -(\mu_b + 4\mu/3)\frac{\partial}{\partial x}\left[\left(\int_0^R 2\pi r \mathrm{v}_x^D dr\right)\frac{d}{dx}\ln\rho\right]. \tag{2.34}$$

The velocity $\mathbf{v}^D$ is induced by the density gradient. Thus, when $d\rho/dx = 0$, $\mathbf{v}^D = 0$. Integrating Eq. (2.34) with respect to x then leads to

$$\rho \int_0^R 2\pi r \left(\mathrm{v}_x^D\right)^2 dr = -(\mu_b + 4\mu/3)\left(\int_0^R 2\pi r \mathrm{v}_x^D dr\right)\frac{d}{dx}\ln\rho. \tag{2.35}$$

Thus, the mass flow rate from the density-gradient induced flow and the corresponding mass flux are given, respectively, by

$$\dot{M}_D = \rho \int_0^R 2\pi r \mathrm{v}_x^D dr = -\pi R^2 C_m D_\rho \frac{d\rho}{dx}, \tag{2.36}$$

$$\dot{m}_D = -C_m D_\rho \frac{d\rho}{dx} = -D_m \frac{d\rho}{dx}, \tag{2.37}$$

$$D_\rho = (\mu_b/\mu + 4/3)\nu, \quad \nu = \mu/\rho, \tag{2.38}$$

$$C_m = \frac{2}{R^2}\frac{\left(\int_0^R r\mathrm{v}_x^D dr\right)^2}{\int_0^R r\left(\mathrm{v}_x^D\right)^2 dr}. \tag{2.39}$$

Therefore, the cross-section averaged mass flux $\dot{m}_D$ obeys Fick's law of diffusion with a diffusion coefficient $D_m = C_m D_\rho$. D_ρ is the self-diffusion coefficient in the free space, which is comparable to that from the kinetic theory of gas that gives $D_{11} = 1.3\nu$ [60]. C_m is a shape correction factor caused by a nonuniform velocity profile v_x^D and it is independent of the strength of v_x^D. For a uniform flow, $C_m = 1$, and, for a parabolic profile that does not slip on the tube wall with the form $1 - r^2/R^2$, $C_m = 3/4$.

Physically, the compressibility-driven large-scale flow $\mathbf{v}^D$ is the aftereffect of the attenuated acoustic wave field at large times, as the acoustic wave associated with the startup process evolves into a diffusive field at large time [44,61–63]. It should be emphasized that the mass flux diffusive law (2.37) is derived from the compressible Navier-Stokes equations. Thus, the self-diffusion effect is already embedded in the classical Navier-Stokes formulation for compressible flow in small capillaries. Self-diffusion of a compressible fluid generates an equivalent body force in the bulk of the fluid: the dilatation term $(\mu_b + 4\mu/3)\nabla(\nabla\cdot\mathbf{v})$ in the momentum equation is directly related to the density gradient, as it can be expressed as $-\nabla(D_\rho D\rho/Dt)$ after using the continuity equation (with D/Dt being the substantial derivative). This term is equivalent to a body force that only manifests itself at a length scale comparable to the length of the tube. This body force is proportional to the fluid's local kinematic viscosity, and for transient flow in linear acoustics it causes a damping of the acoustic wave. For steady-state flow, the equivalent body force becomes $-\nabla(D_\rho \mathrm{v}_x d\rho/dx)$ and it drives a diffusive flow field described by the mass flux Eq. (2.37), which is maintained by the balance of this body force with the convective acceleration at the large length scale. Such a diffusive motion is completely absent in an inviscid compressible flow or an incompressible flow. This dual effect of viscosity (which drives the diffusive flow) also occurs in acoustic streaming [64]. Convection with a nonuniform velocity only modifies the self-diffusion coefficient.

A similar mass diffusive law can be derived for microflows in a channel with a thin gap $2h$ and a large width w ($h/w \ll 1$). The velocity is given by

$$\mathbf{v} = \mathbf{e_x}\mathrm{v}_x(x, y) + \mathbf{e_y}\mathrm{v}_y(x, y), \tag{2.40}$$

where y is measured from the centerline of the channel and the x axis is along the centerline. The corresponding mass flux is given by

$$\dot{m}_{D,\mathrm{ch}} = \frac{\dot{M}_{D,\mathrm{ch}}}{2wh} = -D_{m,\mathrm{ch}}\frac{d\rho}{dx}, \tag{2.41}$$

with

$$D_{m,\mathrm{ch}} = C_{m,\mathrm{ch}} D_\rho, \tag{2.42}$$

$$C_{m,\mathrm{ch}} = \frac{\left(\int_{-h}^{h} \mathrm{v}_{x,\rho} dy\right)^2}{4h \int_{-h}^{h} \mathrm{v}_{x,\rho}^2 dy}. \tag{2.43}$$

For no-slip flow of the parabolic form $1 - y^2/h^2$, the shape correction factor $C_{m,\mathrm{ch}} = 5/6$.

It should be pointed out that in the 1960s Lund and Berman [34] recognized the importance of self-diffusion in low Mach number viscous compressible flow through a narrow conduit. Such an effect is completely absent in models based on a slip-boundary condition [39]. In the context of modern microfluidics applications, Brenner [32] and Durst *et al.* [33] brought the importance of self-diffusion to the attention of the research community. Our analysis in this section confirms the assertions of these previous works. In addition, the analysis here shows that the self-diffusion effect is already included in the compressible Navier-Stokes equations and no constitutive modification is necessary. In this regard, the ENSE theory can be considered as already embedded in the classical formulation.

III. NO-SLIP FLOW WITH A SLIPLIKE MASS FLOW RATE

As shown in Eq. (2.17), the velocity for a low Mach number flow through a small capillary is the sum of an incompressible field $\mathbf{v}^I$ and a diffusive field $\mathbf{v}^D$. These two velocity fields as well as the mass flow rates are found for flow through a long and narrow circular tube in this section.

A. The incompressible field

The incompressible field $\mathbf{v}^I$ is governed by the incompressible flow equations, which for small Reynolds numbers are reduced to the creeping flow equations

$$\nabla \cdot \mathbf{v}^I = 0, \tag{3.1}$$

$$0 = -\nabla p^I + \mu \nabla^2 \mathbf{v}^I. \tag{3.2}$$

For long and narrow capillaries, the lubrication approximation can be used and the solution of Eqs. (3.1) and (3.2) subject to the no-slip condition is the well-known Hagen-Poiseuille velocity:

$$\mathbf{v}^I = -\frac{R^2}{4\mu} \frac{\partial p^I}{\partial x} (1 - r^2/R^2) \mathbf{e}_\mathbf{x}. \tag{3.3}$$

B. The diffusive field

To find the diffusive field $\mathbf{v}^D$, the Helmholtz decomposition is used to decompose $\mathbf{v}^D$ into two parts, $\mathbf{v}^D = \mathbf{v}^{IR} + \mathbf{v}^{RT}$, as in Eq. (2.23), and $\mathbf{v}^D$ satisfies the no-penetration and no-slip condition on the tube wall. An average diffusive speed $V_D(x)$ can be defined through the mass flux Eq. (2.37):

$$\dot{m}_D = \rho V_D = -C_m \frac{\mu_b + 4\mu/3}{\rho} \frac{d\rho}{dx}. \tag{3.4}$$

Thus,

$$V_D = -C_m \frac{\mu_b + 4\mu/3}{\rho^2} \frac{d\rho}{dx}. \tag{3.5}$$

The irrotational part of $\mathbf{v}^D$ is then

$$\mathbf{v}^{IR} = V_D(x)\mathbf{e_x}. \tag{3.6}$$

The solenoidal part of the velocity satisfies the incompressible creeping flow Eqs. (2.28) and (2.29) and the boundary condition

$$r = R : \mathrm{v}_r^{RT} = 0; \quad \mathrm{v}_x^{RT} = -\mathrm{v}_x^{IR} = -V_D(x). \tag{3.7}$$

The boundary condition (3.7) ensures that the diffusive velocity $\mathbf{v}^D$ satisfies the no-slip condition on the capillary wall. Thus, the solenoidal field $(p^D, \mathbf{v}^{RT})$ is driven by the irrotational flow $\mathbf{v}^{IR}$ via the boundary condition (3.7). The solenoidal velocity $\mathbf{v}^{RT}$ can be conveniently found by using the stream-function-vorticity formulation for an axisymmetric flow, with the stream function $\psi(r, x)$ defined by

$$\mathrm{v}_r^{RT} = -\frac{1}{r}\frac{\partial \psi}{\partial x}, \quad \mathrm{v}_x^{RT} = \frac{1}{r}\frac{\partial \psi}{\partial r}. \tag{3.8}$$

Thus,

$$E^4\psi = 0, \tag{3.10}$$

with

$$E^2 = r\frac{\partial}{\partial r}\left(\frac{1}{r}\frac{\partial}{\partial r}\right) + \frac{\partial^2}{\partial x^2}. \tag{3.11}$$

The boundary condition becomes

$$r = R : \frac{\partial \psi}{\partial x} = 0; \quad \frac{\partial \psi}{\partial r} = -R\, V_D. \tag{3.12}$$

On the centerline, the velocity and the vorticity must be bounded. For long and narrow capillaries, the lubrication approximation can be used to simplify E^2. In addition, the flow rate for the diffusive field must vanish when $d\rho/dx = 0$. The solution for the stream function is then

$$\psi = \frac{V_D(x)}{2} r^2 \left(1 - \frac{r^2}{R^2}\right), \tag{3.13}$$

and the components for the solenoidal velocity are given by

$$\begin{aligned} \mathrm{v}_r^{RT} &= \frac{1}{2} r \left(\frac{r^2}{R^2} - 1\right)\frac{dV_D}{dx}, \\ \mathrm{v}_x^{RT} &= V_D(x)\left(1 - \frac{2r^2}{R^2}\right). \end{aligned} \tag{3.14}$$

Finally, the diffusive velocity field is given by $\mathbf{v}^D = \mathbf{v}^{IR} + \mathbf{v}^{RT} = \mathbf{e_r}\mathrm{v}_r^{RT} + \mathbf{e_x}(V_D + \mathrm{v}_x^{RT})$, which has the components

$$\mathrm{v}_r^D = -\frac{1}{2} r \left(1 - \frac{r^2}{R^2}\right)\frac{dV_D}{dx}, \quad \mathrm{v}_x^D = 2V_D\left(1 - \frac{r^2}{R^2}\right). \tag{3.15}$$

The diffusive velocity (3.15) satisfies the no-slip condition on the wall. When the velocity profile (3.15) is substituted into the shape correction factor Eq. (2.39), we obtain the shape correction factor

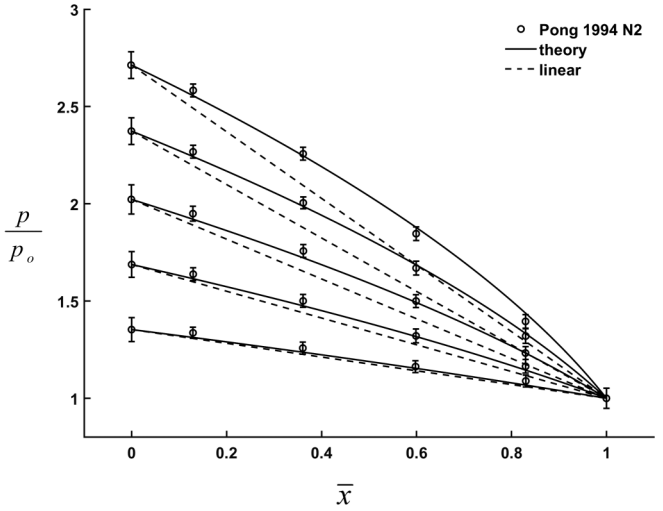

FIG. 2. Comparison of the predicted pressure profiles with the measurements of Pong *et al.* [65], as well as the incompressible flow linear pressure profiles. The five profiles correspond to five different inlet pressures. The outlet pressure is atmospheric.

$C_m = 3/4$, and

$$V_D = -\frac{3\mu_b/4 + \mu}{\rho^2}\frac{d\rho}{dx}. \tag{3.16}$$

The self-diffusion coefficient is then

$$D_m = \frac{3\mu_b/4 + \mu}{\rho}. \tag{3.17}$$

When the bulk viscosity is taken as zero, this diffusion coefficient is reduced to that from the ENSE theory [33].

The above results show that the diffusive velocity field induced by self-diffusion can also satisfy the no-slip condition. This is in contrast to ENSE, which allows the diffusive velocity to slip on the capillary wall.

C. No-slip flow with a sliplike mass flow rate

The total velocity is

$$\mathbf{v} = \mathbf{v}^I + \mathbf{v}^D = -\frac{1}{2}\frac{dV_D}{dx}r\left(1 - \frac{r^2}{R^2}\right)\mathbf{e_r} + \left[-\frac{R^2}{4\mu}\frac{dp}{dx}\left(1 - \frac{r^2}{R^2}\right) + 2V_D\left(1 - \frac{r^2}{R^2}\right)\right]\mathbf{e_x}. \tag{3.18}$$

This velocity profile satisfies the no-slip condition on the tube wall. The volumetric flow rate and mass flow rate are given, respectively, by

$$Q_T = Q_{\mathrm{HP}} + Q_D = -\frac{\pi R^4}{8\mu}\frac{dp}{dx} + \pi R^2 V_D, \tag{3.19}$$

$$\dot{M}_T = \rho Q_T = -\frac{\pi R^4 \rho}{8\mu}\frac{dp}{dx} + \pi R^2 \rho V_D = -\frac{\pi R^4 \rho}{8\mu}\frac{dp}{dx} + \pi R^2 \dot{m}_D. \tag{3.20}$$

Here subscripts T, HP, and D stand for total, Hagen-Poiseuille, and diffusive contributions, respectively. The mass flow rate for the no-slip flow, Eq. (3.20), is the same as that of the slip theory

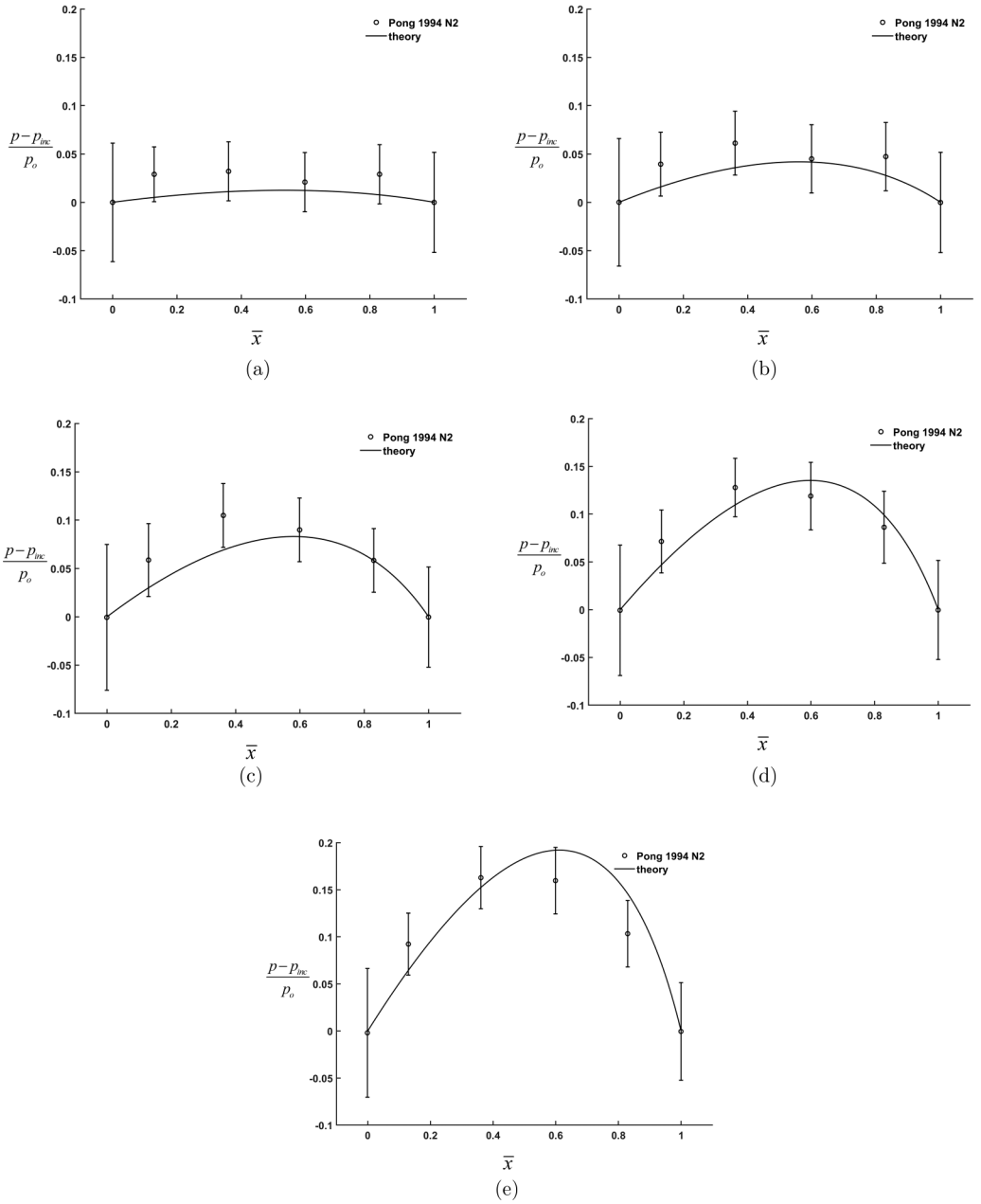

FIG. 3. (a)–(e) Comparison of the pressure deviations from the incompressible pressure with the measurements of Pong *et al.* [65].

of ENSE if the self-diffusion coefficient in ENSE is adjusted to take into account bulk viscosity. Conservation of mass requires the mass flow rate to be a constant. For an ideal gas, $p = \rho \tilde{R} T$, with T being the temperature and $\tilde{R}$ being the gas constant. An equation for the pressure is then obtained:

$$\frac{R^2 p}{8\mu \tilde{R} T} \frac{dp}{dx} + \frac{3\mu_b/4 + \mu}{p} \frac{dp}{dx} = -\frac{\dot{M}_T}{\pi R^2} = \text{const.} \tag{3.21}$$

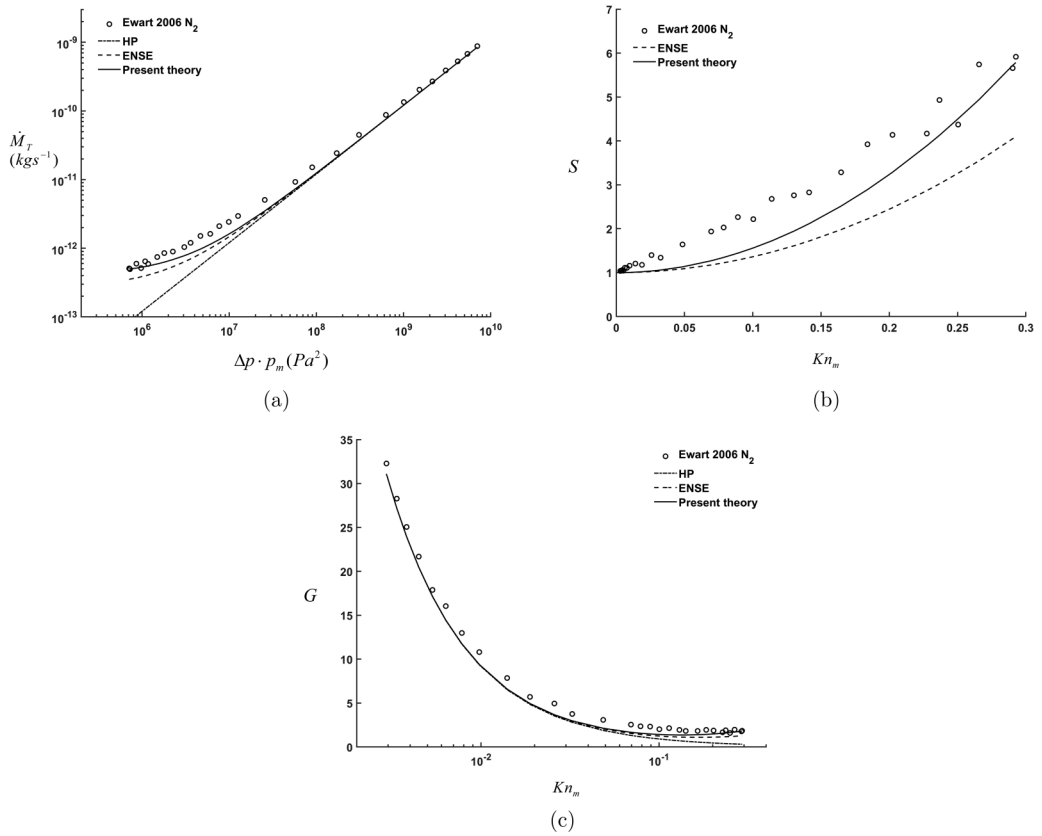

FIG. 4. (a)–(c) Mass flow-rate comparison between theory and the experiment of Ewart *et al.* [17] for nitrogen flow through a microtube. (a) Dimensional mass flow rates in log-log scale. (b) S plots in linear-linear scale. (c) G plots in linear-log scale.

This pressure equation is the same as Eq. (15) of Jaishankar and McKinley [39] after adjusting for the self-diffusion coefficient. The pressure distribution is given implicitly by

$$\bar{p}_i^2 - \bar{p}^2 + \prod_\mu \ln \frac{\bar{p}_i^2}{\bar{p}^2} = \left(\bar{p}_i^2 - \bar{p}_o^2 + \prod_\mu \ln \frac{\bar{p}_i^2}{\bar{p}_o^2} \right) \bar{x}, \tag{3.22}$$

where p_i and p_o are the inlet and outlet pressures, respectively; $\bar{x} = x/L$; $\bar{p} = pR/\mu\sqrt{8\tilde{R}T}$; and $\prod_\mu = 3\mu_b/(4\mu) + 1$. By integrating Eq. (3.21) from the tube inlet to the outlet, the mass flow rate is found:

$$\dot{M}_T = \frac{\pi R^4}{16\mu\tilde{R}T} \frac{p_i^2 - p_O^2}{L} + \pi R^2 \frac{3\mu_b/4 + \mu}{L} \ln \frac{p_i}{p_o}, \tag{3.23}$$

where p_i and p_o are the inlet and outlet pressures. The mass flow rate depends on both the pressure drop and the pressure ratio. The second term is due to self-diffusion, and it provides a sliplike mass flow rate as it is proportional to R^2 instead of R^4 for the Hagen-Poiseuille flow (the first term on the rhs). Equation (3.23) shows that for a very narrow tube the sliplike term dominates, leading to a sliplike mass flow rate for the overall flow.

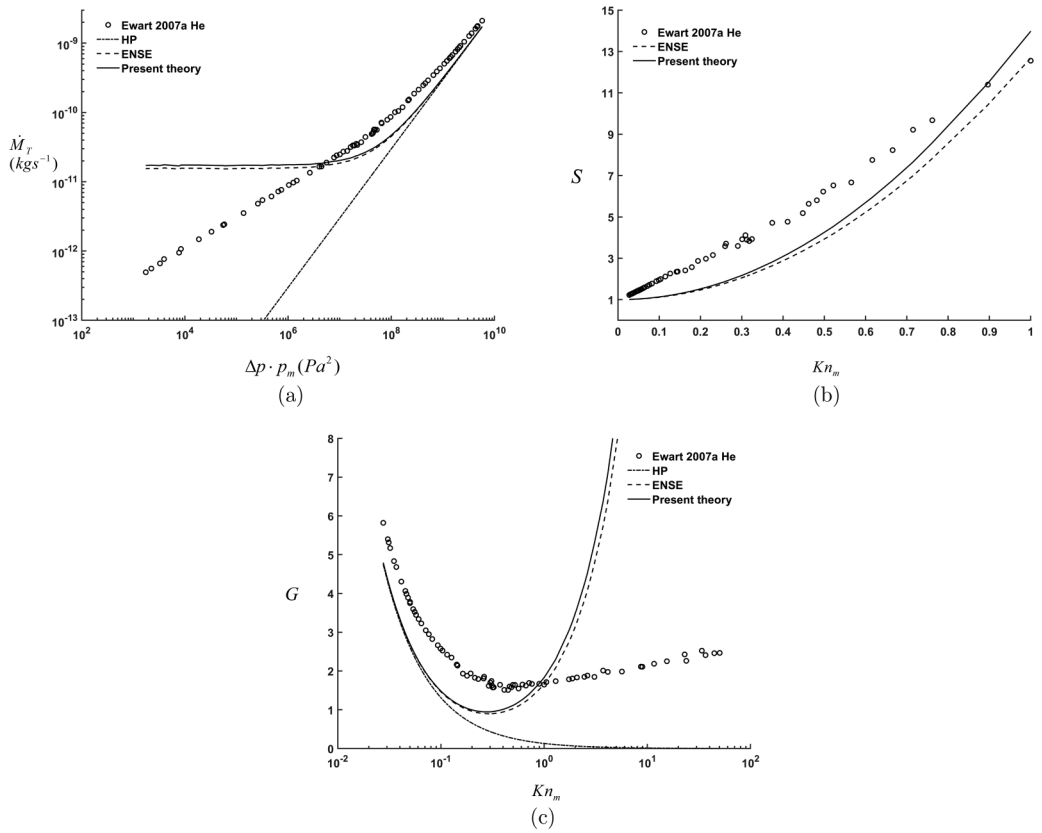

FIG. 5. (a)–(c) Mass flow-rate comparison between theory and the experiment of Ewart *et al.* [18] for helium flow through a microchannel. (a) Dimensional mass flow rates in log-log scale. (b) S plots in linear-linear scale. (c) G plots in linear-log scale.

For channel flow, the overall velocity is

$$\mathbf{v} = \left[-\frac{1}{2\mu}\frac{dp}{dx}(h^2 - y^2) + \frac{3}{2}V_D\left(1 - \frac{y^2}{h^2}\right)\right]\mathbf{e_x} + \frac{y}{2}\left(\frac{y^2}{h^2} - 1\right)\frac{dV_D}{dx}\mathbf{e_y}, \tag{3.24}$$

$$V_D = -\frac{5}{6}\frac{\mu_b + 4\mu/3}{\rho^2}\frac{d\rho}{dx}. \tag{3.25}$$

The pressure is given by Eq. (3.22) with $\bar{p} = ph/\mu\sqrt{3\tilde{R}T}$ and $\prod_\mu = 5\mu_b/(6\mu) + 10/9$. The mass flow rate is

$$\dot{M}_T = \frac{h^3 w}{3\mu L\tilde{R}T}\left(p_i^2 - p_o^2\right) + \frac{2hw(5\mu_b/6 + 10\mu/9)}{L}\ln\frac{p_i}{p_o}. \tag{3.26}$$

IV. COMPARISON WITH EXPERIMENTS

The solution in the previous section is compared to experiments as well as other published works in this section.

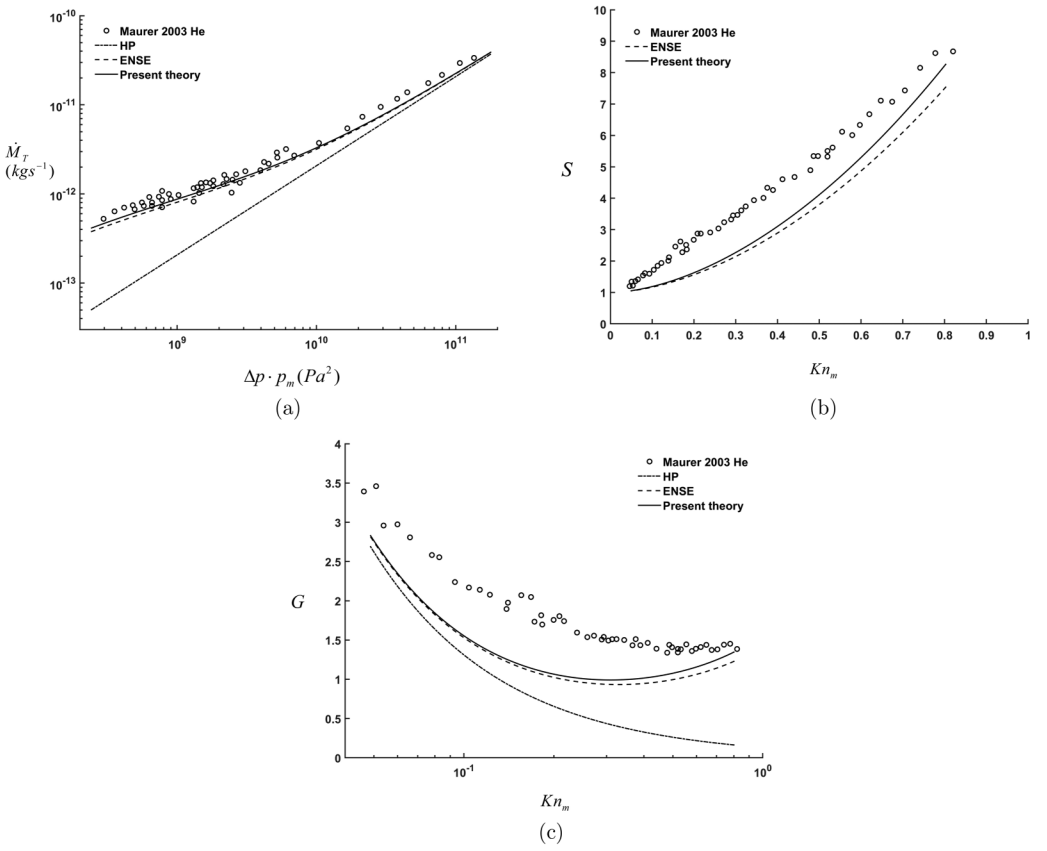

FIG. 6. (a)–(c) Mass flow-rate comparison between theory and the experiment of Maurer *et al.* [15] for helium flow through a microchannel. (a) Dimensional mass flow rates in log-log scale. (b) S plots in linear-linear scale. (c) G plots in linear-log scale.

A. Pressure profile

The theoretical streamwise pressure distribution is compared to the pressure profile measured by Pong *et al.* [65] for the flow of nitrogen through a microchannel (height 1.2 μm, width 40 μm, length 3000 μm) with a fixed outlet pressure p_o of 1 atm and different inlet pressures. Figure 2 shows the dimensionless pressure profile p/p_o for the five sets of measurements with different inlet pressures. The pressure profiles are nonlinear, and the predicted profiles agree very well with the measurements. The deviations from the linear pressure profile of the incompressible flow $(p - p_{\text{inc}})/p_o$ are shown in Figs. 3(a)–3(e). Clearly, the theoretical curves all fall within the error bars of the measurements.

B. Mass flow rate

As noted in the previous section, the mass flow rate for the no-slip flow derived in this paper is the same as that of the slip theory of ENSE when the self-diffusion coefficient in ENSE is adjusted for the contribution from the bulk viscosity. Many authors have previously reported good agreements between ENSE theory and experiments [33,35–39]. These comparisons, however, were mostly carried out by plotting the dimensional mass flow rate $\dot{M}_T$ against $\Delta p \cdot p_m = (p_i^2 - p_o^2)/2$ on log-log scales. A logarithmic scale plot, however, can artificially distort the magnitudes of errors. It is also noted that in studies using Maxwell-type slip-boundary conditions it is customary to plot

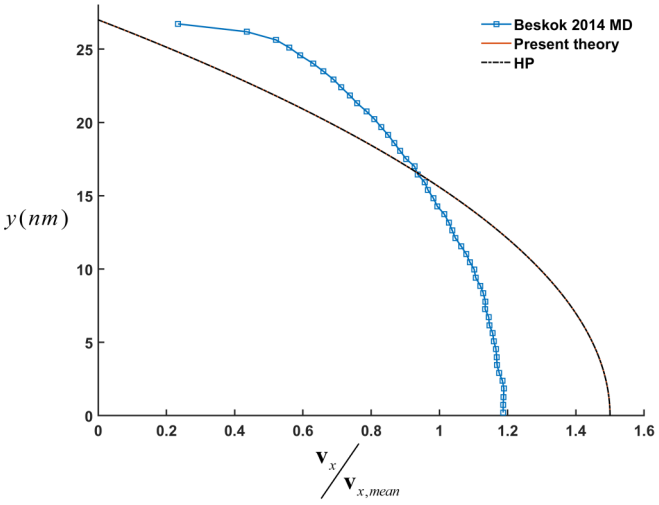

FIG. 7. Streamwise velocity profile in a microchannel flow. The streamwise velocity is normalized by the mean velocity. There is no difference between the normalized velocity from the Hagen-Poiseuille flow and the present theory [they differ dimensionally; see Fig. 8(a)].

dimensionless mass flow rate normalized by the Hagen-Poiseuille rate, $S = \dot{M}_T/\dot{M}_{\rm HP}$, against the mean Knudsen number $\mathrm{Kn}_m = \lambda_m/d$($\lambda_m$ is the average mean free path and d is the tube diameter or the channel height; see the Supplemental Material [66]) on linear scale (the "S" plot). Some authors have also used the Knudsen diffusion mass flow rate $\dot{M}_K = \pi R^3(p_i - p_o)/L\sqrt{2\tilde{R}T}$ for the tube and $\dot{M}_K = (2h)^2 w(p_i - p_o)/L\sqrt{2\tilde{R}T}$ for the channel, to normalize the mass flow rate, $G = \dot{M}_T/\dot{M}_K$ (the "G" plot). In order to provide an unbiased assessment of the mass flow-rate prediction, we use all three types of mass flow-rate plot in the comparison.

In the ENSE literature, the most frequently used experimental data for mass flow-rate comparison are Ewart *et al.* [17] for the tube and Ewart *et al.* [18] and Maurer *et al.* [15] for the channels. The three types of plots for the mass flow-rate comparison between the theory and experiments are shown in Figs. 4(a)–4(c), 5(a)–5(c), and 6(a)–6(c), respectively. A close inspection of these comparisons shows that, while the dimensional mass flow rates on the log-log plots demonstrate reasonably good agreements between the theory (the present theory, or ENSE) and experiment, both S plots and G plots show significant gaps between theoretical predictions and experimental measurements in the slip-flow regime $0.001 < \mathrm{Kn}_m < 0.1$, in which the Navier-Stokes equations are still expected to hold in the bulk of the fluid. This meaningful discrepancy between the predicted mass flow rate and the measured mass flow rate is suppressed by the use of the logarithmic scale in the dimensional mass flow-rate plots. It is noted that the G plot in Fig. 4(c) has much larger values of G than the G plots in Figs. 5(c) and 6(c). Thus, the difference between the theory and the experiments in Fig. 4(c) is actually larger when viewed at the same scale as in Figs. 5(c) and 6(c) (this observation also applies to the G plots in Figs. S1, S3, and S7 in the Supplemental Material [66]). We have also carried out similar comparisons for 32 additional independent experiments [19,21,27,67–79] for both microtubes and microchannels, and they are shown in the Supplemental Material [66]. These additional comparisons confirm the above observation that the theory underpredicts the mass flow rate in the slip-flow regime. Thus, we conclude that the self-diffusion effect is not strong enough to account for the experimentally observed mass flow-rate enhancement from the Hagen-Poiseuille flow solution in the slip-flow regime. This is in stark contrast to the claims made in most of the ENSE publications. The only ENSE publication that mentioned this shortfall is Ref. [38].

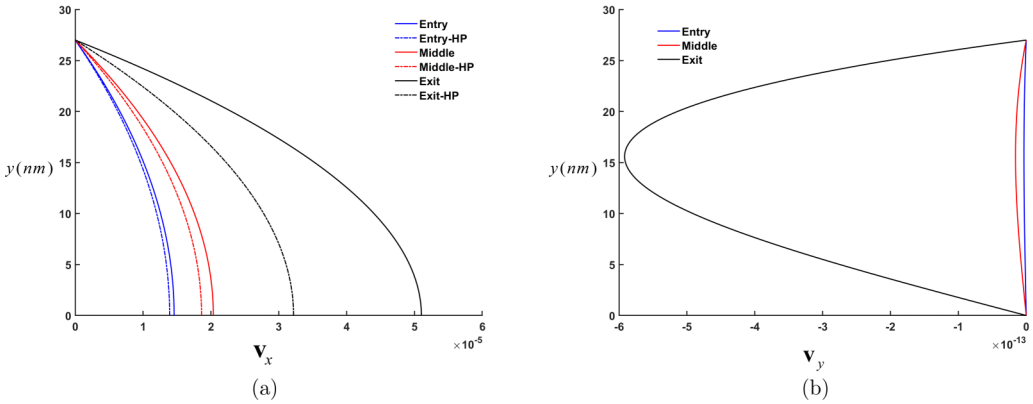

FIG. 8. Streamwise and cross stream velocity profiles in a microchannel flow at the entry, the middle, and the exit sections of the microchannel.

C. Velocity profile

Using molecular dynamics (MD) simulation, Barisik and Beskok [80] computed the velocity profile of the flow of argon through a microchannel with a 54-nm height. The MD simulation converts a pressure-driven flow into a force-driven flow and the streamwise velocity normalized by the mean velocity is shown in their Fig. 4(c) for a modified Knudsen number 0.1. In Fig. 7, the streamwise velocity from the present theory is compared to Fig. 4(c) of Ref. [80]. The normalized velocity from the MD simulation is much fuller than that from the present theory, which could be the reason for the underprediction of the mass flow rate from the present theory in the slip-flow regime. The smaller magnitude of the normalized velocity of MD simulation reflects the fact that its mean velocity is larger than the one from the present theory. Although the Hagen-Poiseuille flow and the present theory have the same normalized velocity, they differ significantly in dimensional terms, as shown in Fig. 8. As shown in Fig. 8(a) for the cross section at the channel entry, the middle, and the exit, the Hagen-Poiseuille flow velocity and the streamwise velocity of the present theory are both parabolic, but they are different parabolas: the self-diffusion effect makes the velocity much larger than that of Hagen-Poiseuille. As the gas moves down the channel, the streamwise velocity increases. Figure 8(b) shows the corresponding y component of the velocity at these cross sections.

V. CONCLUSIONS

The revisit of the classical theory for steady viscous compressible flow through microconduits shows the following:

(i) Contrary to previous claims in the literature, the classical formulation of the compressible Navier-Stokes equations with the no-slip condition includes the self-diffusion (bulk diffusion) effect. Furthermore, the classical formulation also admits a no-slip solution which exhibits a sliplike mass flow rate due to the self-diffusion effect.

(ii) The pressure profile and the mass flow rate of the no-slip solution are the same as those of the ENSE theory when the self-diffusion coefficient is adjusted to take into account the contribution from the bulk viscosity. The ENSE theory, however, introduces an additional constitutive hypothesis and assumes slip at the wall. These additional requirements are not necessary as far as microconduit flow is concerned.

(iii) The predicted pressure profile agrees well with the measured data.

(iv) A more careful and comprehensive comparison with 35 experiments from 19 authors clearly shows that, in the slip-flow regime, the predicted mass flow rate is significantly below the measured flow rate. The self-diffusion effect is too small to account for the observed mass flow-rate

enhancement from the Hagen-Poiseuille solution in the slip-flow regime, contrary to reports in many ENSE publications.

ACKNOWLEDGMENT

We thank the reviewers for their helpful comments and suggestions.

[1] C. M. Ho and Y. C. Tai, Micro-electro-mechanical-systems (MEMS) and fluid flows, Annu. Rev. Fluid Mech. **30**, 579 (1998).
[2] M. Gad-el-Hak, The fluid mechanics of microdevices: The Freeman scholar lecture, ASME Trans. J. Fluids Eng. **121**, 5 (1999).
[3] H. A. Stone and S. Kim, Microfluidics: Basic issues, applications, and challenges, AIChE J. **47**, 1250 (2001).
[4] H. A. Stone, A. D. Stroock, and A. Ajdari, Engineering flows in small devices: Microfluidics toward a lab-on-a-chip, Annu. Rev. Fluid Mech. **36**, 381 (2004).
[5] T. M. Squires, Microfluidics: Fluid physics at the nanoliter scale, Rev. Modern Phys. **77**, 977 (2005).
[6] G. M. Whitesides, The origins and the future of microfluidics, Nature (London) **442**, 368 (2006).
[7] J. C. Maxwell, On stresses in rarified gases arising from inequalities of temperature, Phil. Trans. R. Soc. London **170**, 231 (1879).
[8] M. Knudsen, Die gesetze der molekularstroemung und der inneren reibungsstroemung der gase durch roehren, Ann. Phys. **333**, 75 (1909).
[9] E. B. Arkilic, Gaseous flow in micron-sized channels, Master's thesis, Massachusetts Institute of Technology, 1994, https://dspace.mit.edu/bitstream/handle/1721.1/12321/30998338-MIT.pdf?sequence=2.
[10] C. Harley, Y. H. Huang, H. Bau, and J. N. Zemel, Gas flow in microchannels, J. Fluid Mech. **284**, 257 (1995).
[11] J. Shih, C. Ho, J. Liu, and Y. Tai, Monoatomic and polyatomic gas flow through uniform microchannels, in Proceedings of the ASME Winter Annual Meeting: Application of Microfabrication to Fluid Mechanics, 1996 (unpublished), pp. 197–203.
[12] E. B. Arkilic, M. A. Schmidt, and K. S. Breuer, Gaseous slip flow in long microchannels, J. Microelectromech. Syst. **6**, 167 (1997).
[13] E. B. Arkilic, M. A. Schmidt, and K. S. Breuer, TMAC measurement in silicon micromachined channels, in Proceedings of the 20th Symposium on Rarefied Gas Dynamics, 1997 (unpublished); E. B. Arklic, K. S. Breuer, and M. A. Schmidt, Mass flow and tangential momentum accommodation in silicon micromachined channels, J. Fluid Mech. **437**, 29 (2001).
[14] J. Jang, Y. Zhao, S. T. Wereley, and L. Gui, Mass flow measurement of gases in deep-RIE microchannels, in *Proceedings of the IMECE2002 ASME International Mechanical Engineering Congress Exposition*, IMECE2002-33779, pp. 17–22 (New Orleans, LA, 2002).
[15] J. Maurer, P. Tabeling, P. Joseph, and H. Willaime, Second-order slip laws in microchannels for helium and nitrogen, Phys. Fluids **15**, 2613 (2003).
[16] S. Colin, Rarefaction and compressibility effects on steady and transient gas flows in microchannels, Microfluid. Nanofluid. **1**, 268 (2005).
[17] T. P. Ewart, P. Perrier, I. A. Graur, and J. G. Meolans, Mass flow rate measurements in gas micro flows, Exp. Fluids **41**, 487 (2006).
[18] T. P. Ewart, P. Perrier, I. A. Graur, and J. G. Meolans, Mass flow rate measurements in a microchannel, from hydrodynamic to near free molecular regimes, J. Fluid Mech. **584**, 337 (2007).
[19] T. P. Ewart, P. Perrier, I. A. Graur, and J. G. Meolans, Tangential momentum accommodation in microtube, Microfluid. Nanofluid. **3**, 689 (2007).
[20] C. Cai, Q. Sun, and I. D. Boyd, Gas flows in microchannels and microtubes, J. Fluid. Mech. **589**, 305 (2007).

[21] H. Yamaguchi, T. Hanawa, O. Yamamoto, Y. Matsuda, Y. Egami, and T. Niimi, Experimental measurement on tangential momentum accommodation coefficient in a single microtube, Microfluid. Nanofluid. **11**, 57 (2011).
[22] H.-S. Tsien, Superaerodynamics, mechanics of rarefied gases, J. Aeronaut. Sci. **13**, 653 (1946).
[23] G. Karniadakis, A. Beskok, and N. Aluru, *Microflows and Nanoflows: Fundamentals and Simulation* (Springer, New York, 2005).
[24] E. H. Kennard, *Kinetic Theory of Gases* (McGraw-Hill, New York, 1938).
[25] K. Malek and M. O. Coppens, Knudsen self- and Fickian diffusion in rough nanoporous media, J. Chem. Phys. **119**, 2801 (2003).
[26] A. Beskok and G. E. Karniadakis, Report: A model for flows in channels, pipes, and ducts at micro and nano scales, Microscale Thermophys. Eng. **3**, 43 (1999).
[27] Y. Zohar, S. Y. K. Lee, W. Y. Lee, L. Jiang, and P. Tong, Subsonic gas flow in a straight and uniform microchannel, J. Fluid Mech. **472**, 125 (2002).
[28] N. G. Hadjiconstantinou, Comment on Cercignani's second-order slip coefficient, Phys. Fluids **15**, 2352 (2003).
[29] N. G. Hadjiconstantinou, The limits of Navier-Stokes theory and kinetic extensions for describing small-scale gaseous hydrodynamics, Phys. Fluids. **18**, 111301 (2006).
[30] L. Wu, A slip model for rarefied gas flows at arbitrary Knudsen number, Appl. Phys. Lett. **93**, 253103 (2008).
[31] W. M. Zhang, G. Meng, and X. Wei, A review on slip models for gas microflows, Microfluid. Nanofluid. **13**, 845 (2012).
[32] H. Brenner, Navier-Stokes revisited, Physica A **349**, 60 (2005).
[33] F. Durst, J. Gomes, and R. Sambasivam, Thermofluiddynamics: Do we solve the right kind of equations? in *Proceedings of the International Symposium on Turbulence, Heat and Mass Transfer, Dubrovnik, Croatia, September 25–29* (Begell House, 2006), pp. 3–18.
[34] L. M. Lund and A. S. Berman, Flow and self-diffusion of gases in capillaries. Part II, J. Appl. Phys. **37**, 2489 (1966).
[35] S. Chakraborty and F. Durst, Derivations of extended Navier-Stokes equations from upscaled molecular transport considerations for compressible ideal gas flows: Towards extended constitutive forms, Phys. Fluids **19**, 088104 (2007).
[36] N. Dongari and A. Agrawal, Analytical solution of gaseous slip flow in long microchannels, Int. J. Heat Mass Transf. **50**, 3411 (2007).
[37] N. Dongari, A. Sharma, and F. Durst, Pressure-driven diffusive gas flows in micro-channels: From the Knudsen to the continuum regimes, Microfluid. Nanofluid. **6**, 679 (2009).
[38] S. K. Dadzie and H. Brenner, Predicting enhanced mass flow rates in gas microchannels using nonkinetic models, Phys. Rev. E. **86**, 036318 (2012).
[39] A. Jaishankar and G. H. McKinley, An analytical solution to the extended Navier Stokes equations using the Lambert W function, AIChE J. **60**, 1413 (2014).
[40] T. Veltzke and J. Thaming, An analytically predictive model for moderately rarefied gas flow, J. Fluid Mech. **698**, 406 (2012).
[41] T. Ohwada, Y. Sone, and K. Aoki, Numerical analysis of the shear and thermal creep flows of a rarefied gas over a plane wall on the basis of the linearized Boltzmann equation for hard-sphere molecules, Phys. Fluids A **1**, 1588 (1989).
[42] G. A. Bird, *Molecular Gas Dynamics and the Direct Simulation of Gas Flows* (Clarendon, Oxford, 1994).
[43] M. A. Gallis and J. R. Torczynski, Direct simulation Monte Carlo-based expressions for the gas mass flow rate and pressure profile in a microscale tube, Phys. Fluids **24**, 012005 (2012).
[44] K. P. Chen and D. Shen, Drainage flow of a viscous compressible fluid from a small capillary with a sealed end, J. Fluid Mech. **839**, 621 (2018).
[45] K. P. Chen and D. Shen, Mechanism of fluid production from the nanopores of shale, Mech. Res. Commun. **88**, 34 (2018).
[46] S. Klainerman and A. Majda, Singular limits of quasilinear hyperbolic systems with large parameters and the incompressible limit of compressible fluids, Commun. Pure Appl. Math. **34**, 481 (1981).

[47] S. Klainerman and A. Majda, Compressible and incompressible fluids, Commun. Pure Appl. Math. **35**, 629 (1982).
[48] J. D. Anderson, Jr., *Computational Fluid Dynamics* (McGraw-Hill, New York, 1995).
[49] J. Lighthill, *Waves in Fluids* (Cambridge University, New York,1978).
[50] A. D. Pierce, *Acoustics: An Introduction to its Physical Principles and Applications* (McGraw-Hill, New York, 1981).
[51] P. M. Morse and K. Uno Ingard, *Theoretical Acoustics*, (McGraw-Hill, New York, 1968).
[52] S. Temkin, *Elements of Acoustics* (Wiley, New York, 1981).
[53] K. F. Herzfeld and T. A. Litovitz, *Absorption and Dispersion of Ultrasonic Waves* (Academic, New York, 1959).
[54] R. Klein, Semi-implicit extension of a Godunov-type scheme based on low Mach number asymptotics. I. One-dimensional flow, J. Comput. Phys. **121**, 213 (1995).
[55] C. D. Munz, S. Roller, R. Klein, and K. J. Geratz, The extension of incompressible flow solvers to the weakly compressible regime, Comput. Fluids **32**, 173 (2003).
[56] C. D. Munz, M. Dumbser, and S. Roller, Linearized acoustic perturbation equations for low Mach number flow with variable density and temperature, J. Comput. Phys. **224**, 352 (2007).
[57] R. Aris, *Vectors, Tensors, and the Basic Equations of Fluid Mechanics* (Dover, New York, 1989).
[58] L. G. Leal, *Advanced Transport Phenomena* (Cambridge University, New York, 2010).
[59] R. L. Panton, Incompressible Flow*, 4th ed.* (Wiley, New York, 2013).
[60] J. O. Hirschfelder, C. F. Curtiss, and R. B. Bird, *Molecular Theory of Gases and Liquids* (Wiley, New York, 1954).
[61] M. H. J. Hagen, I. Pagonabarraga, C. P. Lowe, and D. Frenkel, Algebraic Decay of Velocity Fluctuations in a Confined Fluid, Phys. Rev. Lett. **78**, 3785 (1997).
[62] B. U. Felderhof, Transient flow of a viscous compressible fluid in a circular tube after a sudden point impulse, J. Fluid Mech. **644**, 97 (2010).
[63] D. Frydel and H. Diamant, Sound-mediated dynamic correlations between colloidal particles in a quasi-one-dimensional channel. Microparticles in Stokes Flows 2011, J. Phys.: Conf. Ser. **392**, 012007 (2012).
[64] J. W. S. Rayleigh, *The Theory of Sound* (Dover, New York, 1945), Vol. 2.
[65] K. C. Pong, C. M. Ho, J. Q. Liu, and Y. C. Tai, Non-linear pressure distribution in uniform micro-channels. in *Application of Microfabrication to Fluid Mechanics*, vol. 197 of FED (ASME, New York, NY, USA, 1994), pp. 51–56.
[66] See Supplemental Material at http://link.aps.org/supplemental/10.1103/PhysRevFluids.4.024202 for mass flow-rate comparisons for 32 additional independent experiments for both microtubes and microchannels.
[67] J. M. Anderson, M. W. Moorman, J. R. Brown, J. M. Hochrein, S. M. Thornberg, K. E. Achyuthan, and R. P. Manginell, Isothermal mass flow measurements in microfabricated rectangular channels over a very wide Knudsen range, J. Micromech. Microeng. **24**, 055013 (2014).
[68] E. Arkilic, K. Breuer, and M. Schmidt, Mass flow and tangential momentum accommodation in silicon micromachined channels, J. Fluid Mech. **437**, 29 (2001).
[69] I. A. Graur, P. Perrier, W. Ghozlani, and J. G. Méolans, Measurements of tangential momentum accommodation coefficient for various gases in plane microchannel, Phys. Fluids **21**, 102004 (2009).
[70] M. Hadj Nacer, I. Graur, and P. Perrier, Mass flow measurement through rectangular microchannel from hydrodynamic to near free molecular regimes, La Houille Blanche **4**, 49 (2011).
[71] M. Hadj Nacer, I. Graur, P. Perrier, and J. G.Meolans, Gas flow through microtubes with different internal surface coatings, J. Vac. Sci. Technol. A **32**, 021601 (2014).
[72] V. Hemadri, V. V. Varade, A. Agrawal, and U. V. Bhandarkar, Investigation of rarefied gas flow in microchannels of non-uniform cross section, Phys. Fluids **28**, 022007 (2016).
[73] W. Lee, M. Wong, and Y. Zohar, Microchannels in series connected via a contraction/expansion section, J. Fluid Mech. **459**, 187 (2002).
[74] W. Lei and D. R. McKenzie, Revisiting Maxwell's accommodation coefficient: A study of nitrogen flow in a silica microtube across all flow regimes, Ann. Phys. (NY) **351**, 828 (2014).

[75] P. Perrier, I. A. Graur, T. Ewart, and J. G. Méolans, Mass flow rate measurements in microtubes: From hydrodynamic to near free molecular regime, Phys. Fluids **23**, 042004 (2011).
[76] J. Pitakarnnop, S. Varoutis, D. Valougeorgis, S. Geoffroy, L. Baldas, and S. Colin, A novel experimental setup for gas microflows, Microfluid. Nanofluid. **8**, 57 (2010).
[77] M. Rojas-Cárdenas, E. Silva, M. T. Ho, C. J. Deschamps, and I. Graur, Time-dependent methodology for non-stationary mass flow rate measurements in a long micro-tube, Microfluid. Nanofluid. **21**, 86 (2017).
[78] E. Silva, M. Rojas-Cardenas, and C. J. Deschamps, Experimental analysis of velocity slip at the wall for gas flows of nitrogen, R134a, and R600a through a metallic microtube, Int. J. Refrig. **66**, 121 (2016).
[79] A. E. Velasco, S. G. Friedman, M. Pevarnik, Z. S. Siwy, and P. Taborek, Pressure-driven flow through a single nanopore, Phys. Rev. E **86**, 025302(R) (2012).
[80] M. Barisik and A. Beskok, Scale effects in gas nano flows, Phys. Fluids **26**, 052003 (2014).